Hydrolytic resistance of K_2O-PbO-SiO_2 glasses in aqueous and high-humidity environments

T. Palomar*, J. Mosa, M. Aparicio

Instituto de Cerámica y Vidrio, Consejo Superior de Investigaciones Científicas (ICV-CSIC), c/ Kelsen 5, Campus de Cantoblanco, 28049 Madrid, Spain

*Corresponding author, e-mail: t.palomar@csic.es (T. Palomar)

Abstract

Some historical glasses (lead-wood ash glasses, lead-crystal glasses…) are silicate glasses with high content of lead and potassium. This work presents the evaluation of the chemical stability of high-lead glasses in a high relative humidity atmosphere and as result of aqueous immersion. In both situations, the alteration mechanism begins with the lixiviation of alkali metal and lead ions, followed by the hydrolytic attack of the silica glass network. According to the results, the glasses with a higher content of lead show the fastest degradation due to their higher hygroscopicity. Environmental CO_2 can be dissolved in the adsorbed water and favor the formation of intermediate degradation compounds.

Keywords

Lead silicate glasses, degradation, hydrolytic attack, humidity.

1. Introduction

Lead glasses have been used throughout history to produce small objects such as beads, mosaic tiles or rings [1-5], as well as in the decoration of rings, bracelets or small vessels [6-11]. These glasses generally are opaque due to the precipitation of lead antimonate or lead stannate during the glass batch and the annealing [10, 12]. During the medieval period, the production of lead-rich glasses increased in Europe together with plant-ash glasses [4, 5, 13-16]. It was in the late 17th century, when lead-silicate glasses were largely produced to make glass vessels and other luxury objects. The recipes remained secret for around a century before they were produced in northern Europe [17, 18]. The addition of lead oxide to the batch glasses reduces their melting point, which result in cost saving because they would need less wood or coal to maintain the furnace temperatures [4]. It also increases the refractive index of the glass, in other words, their optical properties were more similar to quartz crystal than glasses with other chemical compositions [4, 14, 15, 19, 20]. Due to their lower melting temperature (900-1000 °C), lead-silicate glasses were also used to glaze pottery [21, 22] and as raw material for grisailles and enamels [23-26].

According to their chemical composition, most of the ancient high-lead glasses had lead as the only flux. Heraclius, in the "De coloribus et artibus romanorum" (10th–13th century) stated that high-lead glasses were prepared by two parts of lead oxide and one part of sand [27]. However, to produce high-quality glasses without excessive weight or an expensive content of lead, artisans began to produce lead glasses in combination with supplementary alkali fluxes. Most commonly used fluxes in glasses from central and eastern Europe was the wood ash, which increases the content of potassium in the glasses [20]. In the 17th century, in England, wood ashes were substituted by saltpeter (potassium nitrate) from India to have higher control of the raw materials. This favored the formulation of a new glass composition that was called lead-crystal glass. This glass was patented by George Ravenscroft in 1674 under the title "a perticuler sort of chritaline glasse resembling rock christall" [19, 20]. To develop this new glass composition, glaziers tried several formulations, some of them were finally rejected because of their chemical instability. Some of these unstable formulations had a low content of stabilizer oxides (< 5 wt. % of CaO or MgO), that produced different degradation pathologies in lead-crystal glasses after some years, such as solarizing or crizzling [17, 20, 28, 29].

The degradation mechanism of high-lead glasses (> 40 wt. %) has been studied in acidic conditions [30-36], mainly to avoid the poisoning by lead as a consequence of drinking wine (0.1-0.3 g/l acetic acid [37]) in lead-crystal vessels [30-32, 38]. However, there is not a systematic study about the alteration of these glasses in humid atmospheres, as happens in some collections of

historical glasses without the correct preventive conservation measures or exposed to external environments. This research aims to evaluate the chemical stability of high-lead glasses in high-humidity environments and aqueous immersion in order to study the alteration mechanism, identify the most vulnerable glasses, and contribute to the establishment of the best conservation measures in museums and collections for objects with these chemical compositions.

2. Materials and methods

2.1. Glass samples

Four lead-silicate glasses were formulated in the laboratory with a progressive increase in the PbO content (Table 1). The chemical composition of these glasses was chosen based on historical glasses; Pb15.30 and Pb15.40 represent high-lead glasses used in utilitarian objects [14, 39] and Pb15.50 and Pb15.60 are examples of very high-lead glasses identified in glass wastes or decoration [4, 40].

Table 1. Chemical composition of the model glasses by XRF. Error in brackets

	wt. %			mol. %		
Glass	K_2O	SiO_2	PbO	K_2O	SiO_2	PbO
Pb15.30	16	54.4	29.5	14.1	75.0	10.9
	(0.5)	(2.2)	(0.9)	(0.4)	(3.0)	(0.3)
Pb15.40	15.6	42.9	41.4	15.5	67.0	17.4
	(0.3)	(1.3)	(1.7)	(0.3)	(2.0)	(0.7)
Pb15.50	15.8	32.7	51.5	17.8	57.7	24.5
	(0.6)	(1.1)	(1.0)	(0.7)	(2.0)	(0.5)
Pb15.60	15.4	23.6	60.9	19.7	47.4	32.9
	(0.5)	(0.7)	(1.8)	(0.6)	(1.4)	(1.0)

The raw materials were melted between 1000 and 1375 °C, depending on the glass, during 2 h and then annealed at 350 °C for Pb15.30 and Pb15.40, and at 150 °C for Pb15.50 and Pb15.60.

The obtained glasses were cut to obtain a piece of 10 × 10 × 10 mm, and the rest were ground and sieved to obtain the powder fractions of diameter < 300 µm, 300-500 µm, and > 500 µm. The pieces were embedded in polymeric resin and polished using emery paper and diamond paste to obtain optical quality in the cross section.

2.2. Laboratory corrosion tests

Three accelerated artificial corrosion tests were developed to characterize the interaction of the lead-silicate glasses with water. Two of the tests were made in a desiccator whose bottom was filled with distilled water to fix the relative humidity (RH) at ~100 %. In the desiccator, both powdered glass (< 300 µm) in porcelain weight boats and polished cross-section embedded in resin were exposed for 10 days. Both porcelain weight boats and resin showed a low capacity of water adsorption, in both cases the weight increase due to water adsorption was lower than 0.03 wt. % after 3 days at the test conditions. The conditions inside the desiccator were monitored with a data logger for humidity and temperature (HL-1D by Rotronic measurement solutions).

The third test was made in an oven according to the Standard ISO 719:1985 [41] to measure the hydrolytic resistance of glass grains at 98 °C. According to the standard, 0.5 g of powdered glass (300-500 µm) was put in polypropylene tubes with 5 ml of distilled water. The tubes were kept inside the oven at 98 °C during 1, 3, 5, and 10 h. Then the solution was filtered to analyze both the solid and the liquid fraction.

2.3. Characterization techniques

Glass samples were characterized by the following techniques: gravimetry, X-ray fluorescence spectroscopy (XRF), inductively coupled plasma coupled with optical emission spectrometry (ICP-OES), Field Emission Scanning Electron Microscopy (FE-SEM), measurement of the contact angles, µ-Raman confocal spectroscopy, Fourier Transform Infrared Spectroscopy in Attenuated Total Reflectance mode (FTIR-ATR) and X-ray diffraction (XRD).

The mass variation was evaluated using an A&D Instruments analytical balance, model GR-200-EC. Grounded glass was weighed after each test to determine the mass loss (Eq. 1).

$$\Delta weight\ (\%) = \frac{(weight_{altered} - weight_{original})}{weight_{original}} \qquad \text{(Eq. 1)}$$

The chemical composition of the glasses before exposure was analyzed by XRF. The measurements were carried out with a PANalytical MagicX (PW-2424) wavelength dispersed X-ray spectrometer equipped with a rhodium tube (SUPER SHARP) of 2.4 KW. Analytical determinations were undertaken through the analysis with control standards of natural minerals from British Chemical Standards (BCS) and National Institute of Standards Technology (NIST), and a powder sample prepared in a fused pearl. A Philips Perl'X3 equipment was employed for making pearl samples using a platinum-gold crucible. Pearls were melted at 1050 °C from a

homogeneous mixture of 0.3 g of the powder sample (< 75 µm) and 5.5 g of anhydrous $Li_2 B_4O_7$ and LiBr.

Filtered liquids without any other preparation were analyzed by ICP-OES, Agilent ICP-OES 720 coupled to an echelle polychromator and a simultaneous CCD detector. This equipment measures in the whole range of wavelengths (167-770 nm).

Morphological analysis of the glass surfaces were performed by Field Emission Scanning Electron Microscopy (FE-SEM) HITACHI S-4700. For elemental chemical analysis by Energy Dispersive X-ray Spectroscopy (EDX) a NORAN system six was connected to the FE-SEM.

Contact angle measurements between the glass samples and distilled water were performed using the Easy Drop Standard "Drop Shape Analysis System" Kruss DSA 100 measurement apparatus under ambient laboratory conditions with the aim of evaluating the wettability of the original glass samples. The contact angle of each glass was measured at least three times, and the average value and standard deviation were calculated.

Raman spectra were recorded using a confocal Raman microscope integrated with atomic force microscopy (AFM) on a CRM-Alpha 300 RA microscope (WITec, Ulm, Germany) equipped with a Nd:YAG dye laser operating at 532 nm and a X100 objective lens (NA ¼ 0.9). The incident laser power was 5 mW and the Raman spectral resolution was down to 0.02 cm^{-1}. The sample was mounted on a piezo-driven scan platform with 4 nm lateral and 0.5 mm vertical positional accuracy. The piezoelectric scanning table allows steps of 3 nm (0.3 nm in the vertical direction), giving a very high spatial resolution for both the AFM and the CRM. The superficial selected areas studied were 10 µm x 10 µm and the acquisition time was 0.05 s for one single spectrum. Collected spectra were analyzed using Witec Control Plus software.

The measurements of Fourier transform infrared spectroscopy (FTIR) were measured by a Spectrum 100 FT-IR Spectrometers of Perkin Elmer with a diamond crystal detector. Manual pressure accessory was used to ensure good contact between glass and crystal. The measurements were obtained in Attenuated Total Reflection (FTIR-ATR) mode with a spectral range from 4000 to 400 cm^{-1} and a spectral resolution of 4 cm^{-1}. Each spectrum was the product of 8 internal scans.

X-ray powder diffraction data were collected over the range $5° \leq 2\theta \leq 70°$ in a step width of 0.05° and a counting time of 1s per step employing a Bruker D8 Advance diffractometer (BRUKER, Billerica, MA, USA) equipped with a solid-state rapid LynxEye detector, and monochromatic Cu Kα1 radiation.

3. Results

3.1. Glass behavior in atmosphere ~100 % RH

To evaluate the wettability of high-lead glasses, the contact angle between the glass surface and water drops was measured before the alteration tests. This property was similar in the four glasses independent of the glass composition (Table 2), which indicates that the water droplets have the same behavior in the different glass surfaces and the subsequent glass alteration depends on the stability and hygroscopicity of each glass and not on their wettability [42].

Table 2. Average of contact angle values and standard deviation for droplets of distilled water on the glass surfaces.

Glass	Contact angle (°)
Pb15.30	40.0 ± 4.4
Pb15.40	34.8 ± 3.8
Pb15.50	39.6 ± 2.7
Pb15.60	41.4 ± 5.7

Glass powder (Ø < 300 μm) from the four lead-silicate glasses was exposed to a ~100 % RH atmosphere and resulted in a progressive increase in mass in all samples (Fig. 1). The data suggests that there is a relation between the content of lead and the adsorption of environmental humidity. The higher hygroscopicity of the glass Pb15.60 resulted in the presence of visible liquid in the container after three days of exposure. This liquid increased the weight of the glass doubling it in four days and, after 10 days, the weight was around the triple (Fig. 1). On the contrary, the weight of the glasses Pb15.30 and Pb15.40 just increased ~10 % due to their lower hygroscopicity. After 10 days, they did not present visible liquid in their containers. The aqueous solution in contact with the glasses Pb15.50 and Pb15.60 presented a very high pH, in both cases around pH 11. The FTIR-ATR analyses of the solutions confirm that they are aqueous solutions with a small concentration of carbonate ions (Fig. 2). These ions, which were not present in the glass, are the result of the dissolution of environmental CO_2 in the solution adsorbed on the glass surface.

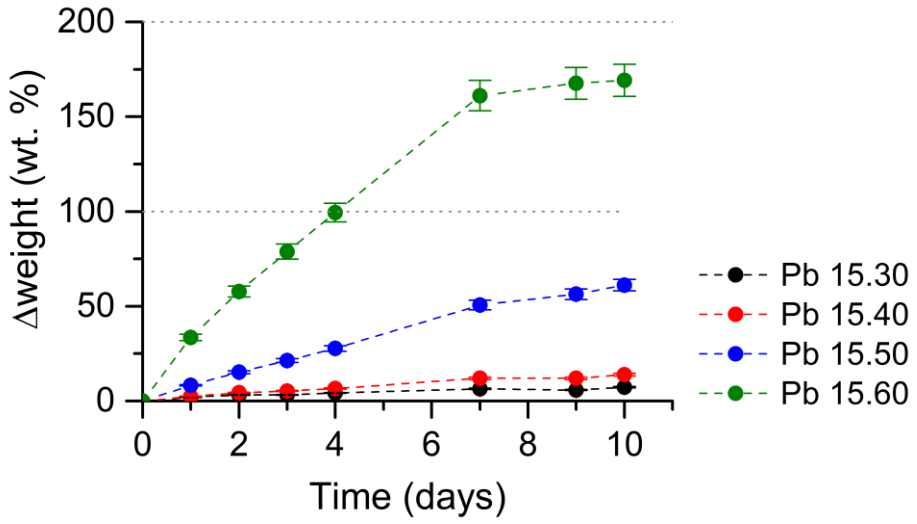

Fig. 1. Mass variation of grounded glass (Ø < 300 µm) as a function of time (Eq. 1)

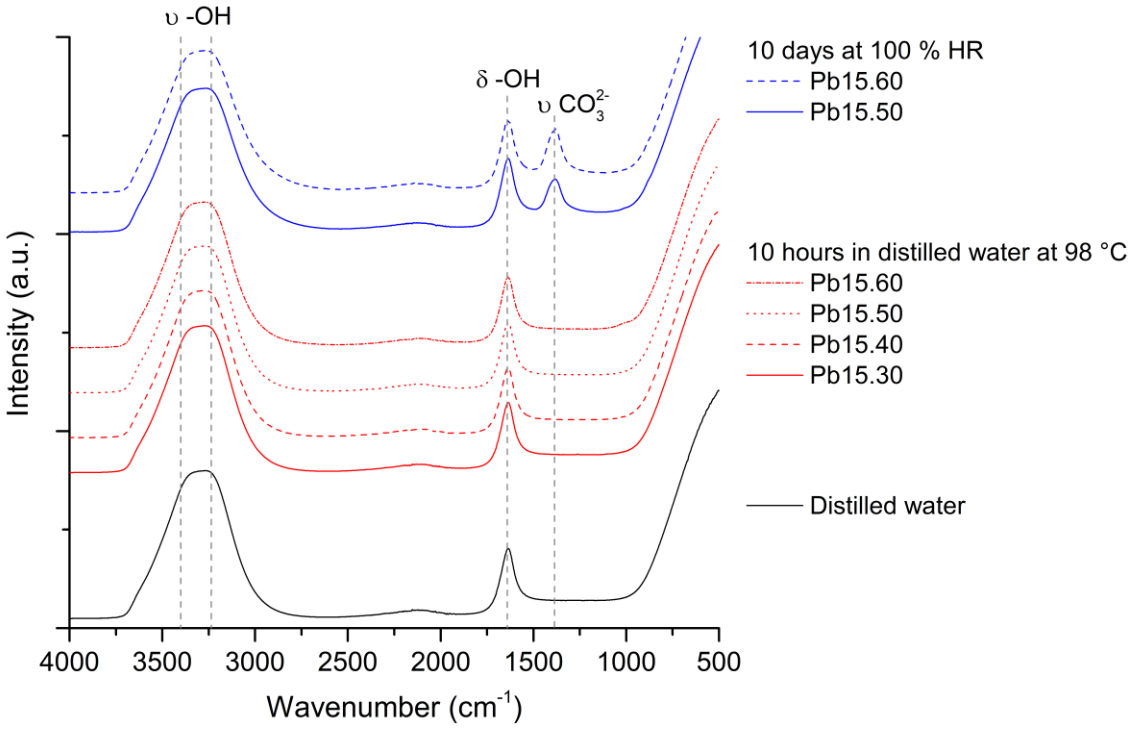

Fig. 2. FTIR-ATR spectra of distilled water, the final solutions of the hydrolytic resistance test, and the liquid adsorbed to the glass powder after 10 days at ~100 % HR. Types of vibrations: υ: stretching; δ: bending.

After the 10 days of test, the grounded glasses were filtered and dried at 75 °C for 5 h. The XRD analyses of the solids show the broad band of the glass in the four cases, and the diffraction peaks of $2PbCO_3 \cdot KOH$ in the samples Pb15.50 and Pb15.60 (Fig. 3).

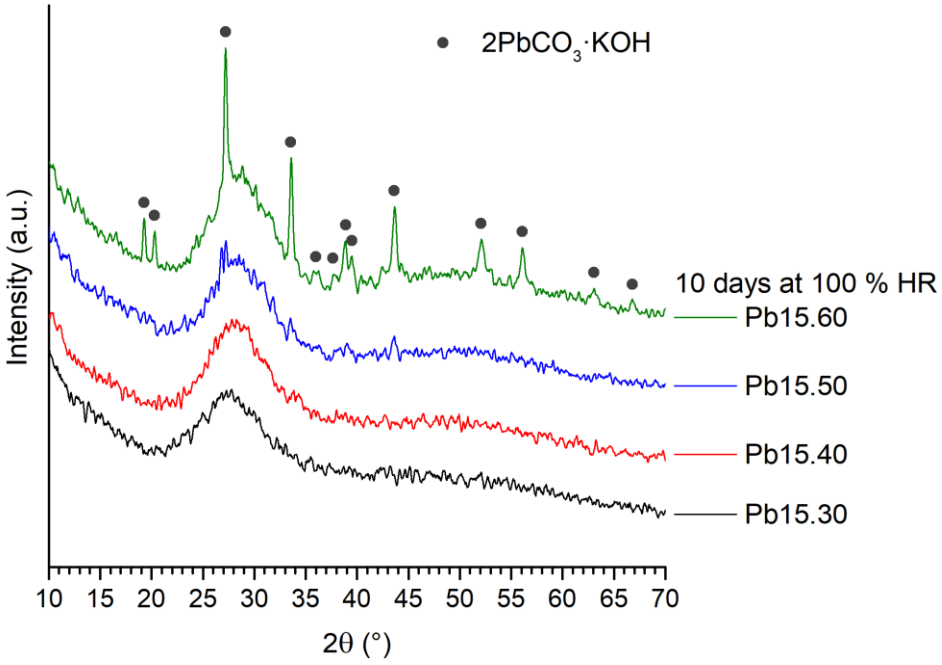

Fig. 3. XRD spectra of the solid phase after 10 days at ~100 % HR.

Glass coupons were also exposed to the same conditions as grounded glasses (desiccator at ~100 % RH). Pb15.30 was almost stable to the alteration after 10 days at high humidity because the surface just shows the formation of isolated deposits (Fig. 4 a and b), but they are homogeneously distributed on Pb15.40 glass surface (Fig. 4 c and d). The glass Pb15.50 shows a cracked surface with detached areas (Fig. 4 e) and several deposits on the most altered areas (Fig. 4 f). These deposits are flat and perpendicular to the surface as result of their growth. The most altered glass is Pb15.60. After the 10 days of the test, the coupon shows an irregular surface, which was fragile and easily breakable under little pressure due to the high concentration of cracks (Fig. 4 g). Big crystals (> 5 µm) are also observed on the surface of the most altered areas (Fig. 4 h). This glass experienced also a significant increase of volume (3 mm in 3 days) due to the adsorption of environmental humidity and formation of the alteration layer.

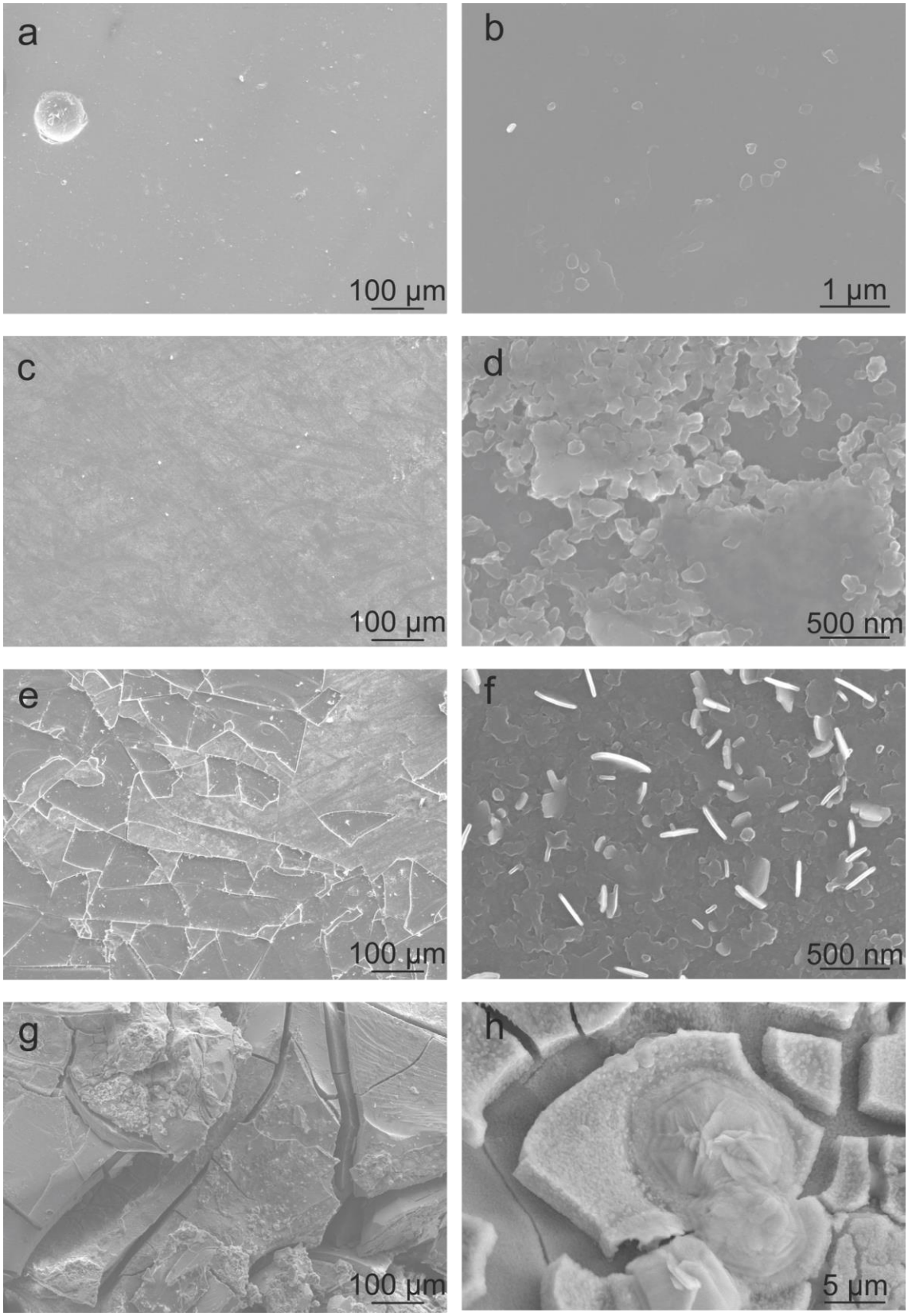

Fig. 4. SEM images of the glass surface a-b) Pb15.30, c-d) Pb15.40, e-f) Pb15.50, and g-h) Pb15.60, after being exposed during 10 days at ~100 % RH.

The µ-Raman analysis of the surface of the glass Pb15.60 after 3 days at ~100 % RH does not show the Raman bands of carbonates, such as in the glass powder, but an increase in the bending bands and the stretching bands Q1 and Q2 of the glass (Fig. 5, Table 3), which are related to the presence of silica linked to a one oxygen atom (Q1) or two oxygen atoms (Q2) [43]. This structure is common in the silica gel layer (alteration layer).

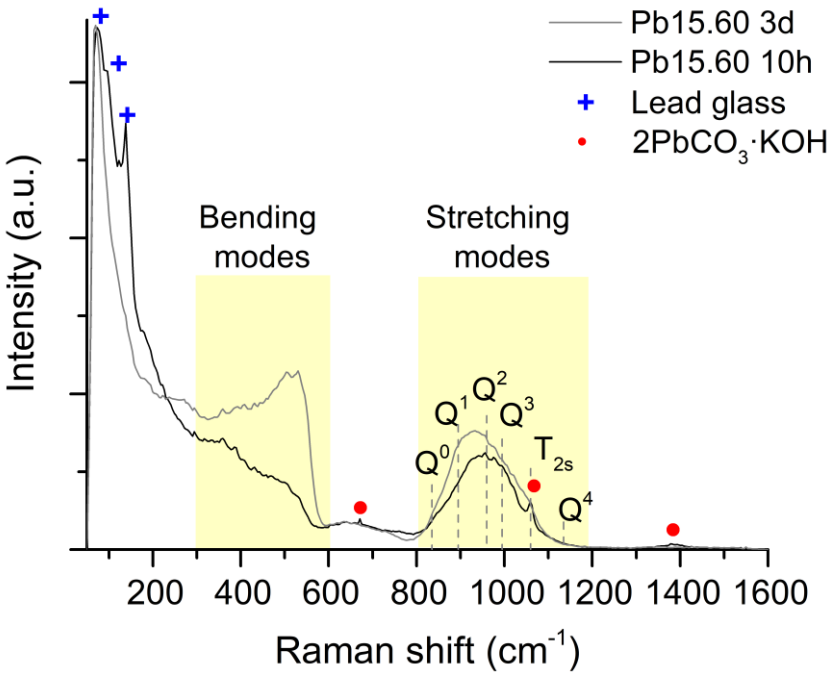

Fig. 5. µ-Raman spectra of the Pb15.60 glass surface after 3 days at ~100 % HR in environmental temperature and Pb15.60 glass powder immersed in distilled water for 10 hours at 98 °C.

Table 3. Main assignments of Raman bands detected on the surface of Pb15.60 glass after the corrosion tests (Fig. 5).

Raman shift (cm^{-1})	Assignment	Related to:	References
71	"Boson" peak	Lead glass	[27]
94	Ionic Pb-O bond	Lead glass	[27-29]
138	υ_{sym} Pb-O	Lead glass	[27, 29]
300-600	Bending modes of silicate glass	Silicate glass	[26, 30]
682	υ_4-in-plane band of CO_3^{2-} groups	$2PbCO_3 \cdot KOH$	[31, 32]
800-1300	Stretching modes of silicate glass	Silicate glass	[26, 29, 30]
1057	υ_1-symmetric C–O stretching of CO_3^{2-} groups	$2PbCO_3 \cdot KOH$	[31, 32]
1386	υ_3-asymmetric C–O stretching of CO_3^{2-} groups	$2PbCO_3 \cdot KOH$	[31, 32]

The surface of the glass coupons was also daily monitored by FTIR-ATR. After one day of test (Pb15.60 d1), it is observed the increase in the hydroxyl, bicarbonate and carbonate bands in comparison to the original glass (Pb15.60 d0) (Fig. 6, Table 4). After three (Pb15.60 d3) and five (Pb15.60 d5) days, the hydroxyl band maintains its intensity; in contrast to the bicarbonate

bands, whose intensity decreases in favor of the carbonate ions and the bands related to the $2PbCO_3 \cdot KOH$ (Fig. 6). The characteristic values of the main bands for FTIR-ATR modes are summarized in Table 4.

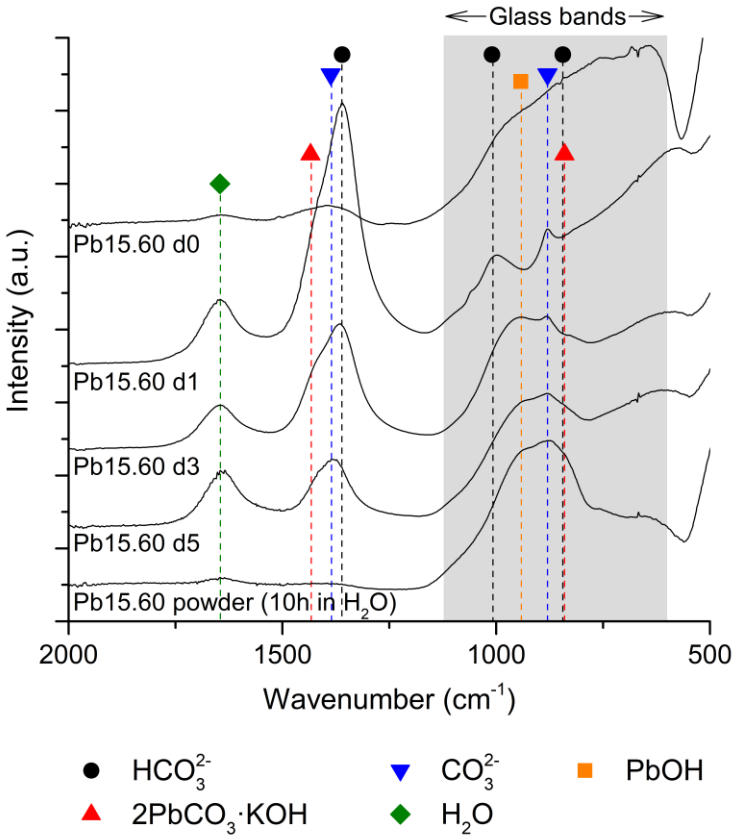

Fig. 6. FTIR-ATR spectra of the Pb15.60 glass surface at different times.

Table 4. Main assignments of FTIR-ATR bands detected on the surface of Pb15.60 glass after the corrosion tests (Fig. 6).

IR band (cm^{-1})	Assignment	Related to:	References
60	υ_3-asymmetric C–O stretching of CO_3^{2-} groups	HCO_3^-	[31,33]
618-605	Symmetric stretching vibration Si-O-Si	Glass	[34]
754-762	Asymmetric stretching vibration Si-O-Si Asymmetric stretching vibration Si-O-Pb	Glass	[34]
840	υ_2 asymmetric C–O	$2PbCO_3 \cdot KOH$	[32]
844	CO_3 out-of-plane bending vibration	$KHCO_3$	[35-37]
855-927	Asymmetric stretching vibration Si-O^-	Glass	[34]
942	δ PbOH	PbOH	[32]
971	Asymmetric stretching vibration Si-O-Si	Glass	[34, 38]
1010	υ_5 (stretching of C-OH) at	HCO_3^-	[35-37, 39]
1121-1054	Asymmetric stretching vibration Si-O-Si	Glass	[34]
1360-1365	υ_3 (symmetric stretching of CO_2)	HCO_3^-	[35-37, 40, 41]
1385	CO_3^{2-}	CO_3^{2-}	[40, 41]
1413, 1430	υ_3 asymmetric C–O	$2PbCO_3 \cdot KOH$	[32]
1645	Bending modes of H-O-H	H_2O	[34]

3.2. Glass behavior in aqueous solution

To evaluate the hydrolytic resistance of the high-lead glasses, glass powder (300 < Ø < 500 µm) was immersed in distilled water at 98 °C during 1, 3, 5, and 10 h, according to the standard ISO 719:1985 [41].

After the test, ICP-OES analyses of the aqueous solutions show that all the glasses experienced a progressive depletion in potassium, silica and lead from their glass structure as result of their interaction with the distilled water. The most concentrated specie in the solutions is K^+ (Fig. 7 a) because it experiences a quick ion-exchange with the H^+ from the water. This exchange also induces a progressive increase of the pH of the solution (Fig. 8). Larger is the duration of the test, higher is the [K^+] leached from the glasses (Fig. 7 a and d), and higher is the pH of the solution (Fig. 8).

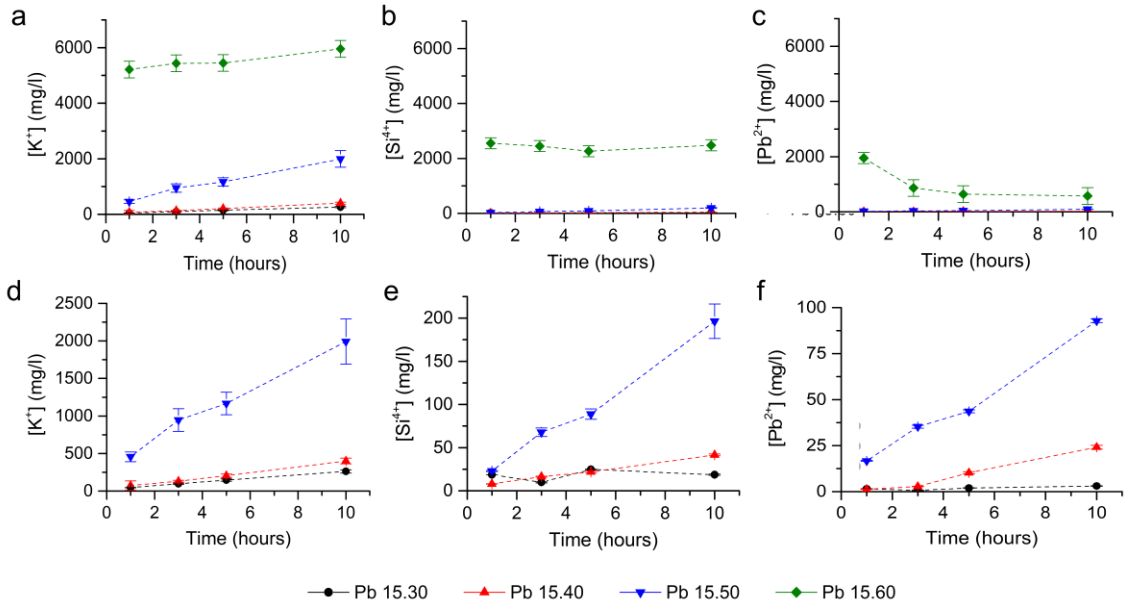

Fig. 7. ICP-OES analyses of the aqueous solutions after the test for the species a,d) [K^+]; b,d) [Si^{4+}]; c,f) [Pb2+]. Results in the graphs d-f are the same than in the graphs a-c, but at different scale.

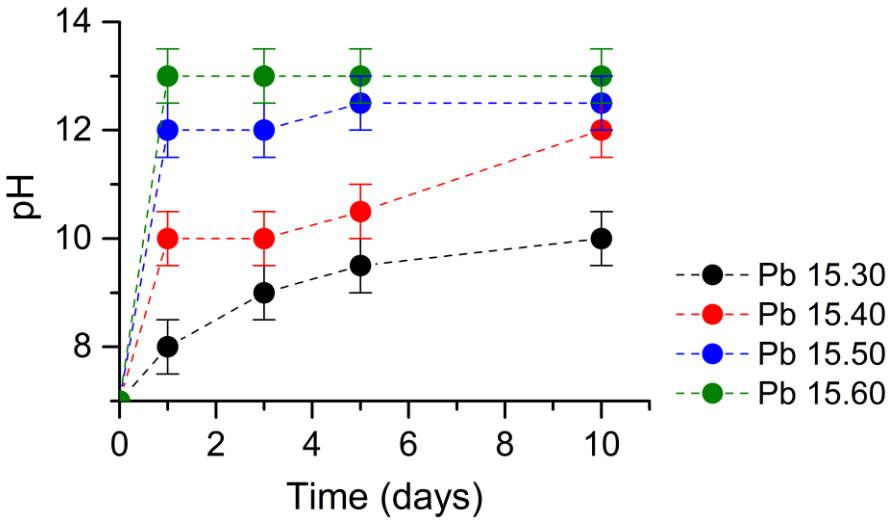

Fig. 8. Evolution of the pH of the solutions during the immersion test.

The second specie most concentrated in the solutions after the test is Si^{4+} (Fig. 7 b). The concentration of Si^{4+} ions after 10 h of test shows three different behaviors (Fig. 7 b and e). In Pb15.30, the silica dissolved in the medium is very low (< 50 mg/l) and constant along the test. The aqueous medium shows a final pH of ~10, which was not enough to dissolve the silica gel layer [44]. The glasses Pb15.40 and Pb15.50 show a progressive increase of the Si^{4+} ions in the medium, as result of the progressive increase of the solution pH. The behavior of Pb15.60 shows a high [Si^{4+}] value after one hour of test and it is almost constant along the experiment (Fig. 7 b). After the first hour, the pH of the medium is ~13. This value favored the silica layer dissolution, but also the formation of a depleted layer with large thickness and lead precipitates that could cause the eventual slowing of the ionic interdiffusion leading to a stable condition [36].

The progressive increase of the pH also induces the lixiviation of lead ions from the glass structure. For the tests with Pb15.30, Pb15.40, and Pb15.50, it is observed a progressive increase up to 100 mg/l after 10 h of test (Fig. 7 f). However, the evolution of the [Pb^{2+}] in Pb15.60 is the contrary (Fig. 7 c and f). Longer was the duration of the tests; lower is the [Pb^{2+}] in the solution. This progressive decrease of [Pb^{2+}] was due to the formation of lead hydroxyl complexes.

Neither of the solutions present carbonate ions (Fig. 2), probably due to the lower duration of the test. However, the Raman bands of hydroxides and $2PbCO_3 \cdot KOH$ are observed together with the bands assigned to lead glass in the solid fraction of the Pb15.60 glass (Fig. 5, Table 3). These compounds could be formed during the drying in the oven after the test.

4. Discussion

4.1. Alteration mechanism

The tests show that all high-lead glasses present the same corrosion mechanism but with different alteration rates depending on their chemical composition.

According to the tests, environmental water adsorbed to the glass surface and the aqueous solution induces the lixiviation of alkali metal (Reaction 1) and lead ions (Reaction 2).

$$\equiv Si\text{-}O\text{-}K + H_2O \rightarrow \equiv Si\text{-}OH + K^+ + OH^- \quad \text{(Reaction 1)}$$

$$\equiv Si\text{-}O\text{-}Pb\text{-}O\text{-}Si\equiv + 2H_2O \rightarrow 2\ (\equiv Si\text{-}OH) + Pb^{2+} + 2\ OH^- \quad \text{(Reaction 2)}$$

As result, K^+ and Pb^{2+} ions from the surface are leached, leaving a hydrated silica layer on the glass surface [32, 35, 36, 45]. The ion-exchange process generates several atomic voids, empty spaces and dissolution channels that form a hydrated silica gel layer on the surface [38]. The rate of this reaction depends on the concentration of K^+ and Pb^{2+} in the glass and their diffusion through the silica gel layer [46]. The ion-exchange between K^+ and H^+ ions (Reaction 1) is more favorable from the energetic point of view than the exchange between Pb^{2+} and H^+ ions (Reaction 2) because less energy is needed to break the [Si-O-K] bond than to break the two bonds in [Si-O-Pb-O-Si]. This agrees with the higher content of K^+ ions in the aqueous medium after the hydrolytic test (Fig. 7 a and d).

Water can also induce the hydrolytic attack of the glass network to form silanol groups (Reactions 3).

$$\equiv Si\text{-}O\text{-}Si\equiv + H_2O \leftrightarrow 2\ \equiv Si\text{-}OH \quad \text{(Reaction 3)}$$

The aqueous solution can enter through the dissolution channels and react with the siloxane bonds. The diffusion inside these layers can produce that the hydroxyl ions generated during the alkali metal leaching (Reaction 1) are leached, increasing the pH of the medium [44, 47]. This increase of hydroxyl ions (pH > 7) is verified in the aqueous tests and in the liquid adsorbed to the glasses Pb15.50 and Pb15.60 after the high-humidity test. The increase of the pH accelerates the breaking of the SiO_2 network through the reaction of dissolution (Reaction 4) [31, 33, 36, 38, 46]. The dissolution of the silica layer is produced predominantly at pH > 9 [44].

$$\equiv Si\text{-}O\text{-}Si\equiv + OH^- \rightarrow \equiv Si\text{-}OH + \equiv Si\text{-}O^- \quad \text{(Reaction 4)}$$

When the glass structure is dissolved, the different ions in the glass network are dispersed in the aqueous solution. The low content of lead in the solutions (< 100 mg/l for Pb15.30, Pb15.40, Pb15.50; and < 1000 mg/l for Pb15.60 for tests longer than three hours) (Fig. 7 c and f) is due to both, its slower capacity of leaching because of their size and its faster reaction with the hydroxyl ions from the medium to form different lead hydroxyl complexes, such as the ionic species $PbOH^+$, $Pb(OH)_3^-$, Pb_2OH^{3+}, $Pb_4(OH)_4^{4+}$ and $Pb_6(OH)_8^{4+}$ and the solid $Pb(OH)_2$. The concentration of each ion depends on the pH value and the total lead concentration [48, 49]. $Pb_6(OH)_8^{4+}$ is dominant in the pH range 8-11. However, in basic conditions, the solid $Pb(OH)_2$ is formed, removing the lead from the solution (Fig. 7 c).

Similar results were observed by Ahmed and Youssof [38]. In their experiments, the concentration of the species lixiviated increases in the order: Si>K>Na>>Pb, but in this study is K>Si>Pb. This difference could be due to both a higher content of potassium in these glasses and a higher glass/water relation that accelerates the corrosion rate [38, 50].

The design of the tests do not include CO_2 or carbonate ions (section 2.2); however, carbonates are identified in the surface of some glasses after being dried in the oven (Fig. 3, 5 and 6). During the tests, environmental CO_2 is probably dissolved in the aqueous medium [51]. At the pH of the adsorbed solution, the CO_2 is in equilibrium with the HCO_3^- specie (Reactions 5 and 6), as it is detected in the Pb15.60 glass surface after one day of test (Fig. 6). At higher pH, the equilibrium favors the formation of carbonates in the medium (Reaction 7), as it is identified in the surface of the Pb15.60 glass after five days of test (Fig. 6) and in the solution adsorbed to the glass powder Pb15.50 and Pb15.60 after 10 days of test (Fig. 2).

$$CO_2 + H_2O \leftrightarrow H_2CO_3 \qquad \text{(Reaction 5)}$$

$$H_2CO_3 + H_2O \leftrightarrow HCO_3^- + H_3O^+ \qquad \text{(Reaction 6)}$$

$$HCO_3^- + OH^- \leftrightarrow CO_3^{2-} + H_2O \qquad \text{(Reaction 7)}$$

The formation of carbonates can induce the precipitation of solid $PbCO_3$. However, the water evaporation increases the concentration of K^+ ions, leached from the glass, and OH^- ions, formed during the alteration, which can react with the carbonates to form the compound $2PbCO_3{\cdot}KOH$, detected by several techniques such as FTIR-ATR (Fig. 6), XRD (Fig. 3) and μ-Raman spectroscopy (Fig. 5). This compound is not formed on the surface of the glass immersed in distilled water because of the short time of the experiment.

4.2. Influence of the composition

In this study, it is observed that Pb15.30 and Pb15.40 presented a similar chemical resistance in the aqueous test (Fig. 7 d and e). The lowest concentration of Pb^{2+} is observed in the aqueous solution for the Pb15.30 glass (Fig. 7 f) due to its higher stability in comparison to the other ones. On the contrary, Pb15.60 is the less resistant glass because their solutions present the highest concentration of K^{+}, Si^{4+} and Pb^{2+} (Fig. 7 a, b and c), the fastest increase of the solution pH (Fig. 8), and the most advanced alteration pathologies (Fig. 4 g and h).

Potassium ions in silicate glasses create non-bridging bonds [≡Si-O-K] that favor the ion-exchange mechanism, leaving big channels of diffusion within the glass [31-33]. Also, the leached alkali favors the hygroscopicity of the glass surface [52], accelerating the adsorption of environmental water to the glass surface, which increases the alteration rate. The content of potassium in the glasses analyzed in this study is similar in wt. %, but it is observed a higher content of alkali metal ions in mol % (Table 1). This means that the relation between the atoms of potassium and silica is higher in the glasses with a higher content of lead, which contributes to their faster degradation. Regarding the lead content, PbO acts as modifier in silicate glasses with low content of lead (< 40 mol. %). For these concentrations, an increase of PbO in the glass induces the decrease in the binding energy of the bonds [-O-Pb-O-] [32, 53], favoring the ion-exchange and, therefore, decreasing their chemical stability [34, 54]. When the concentration of PbO in the glass is higher than 40 mol. %, lead atoms began to be interconnected through polymeric chains of PbO_4 being a former oxide [53, 55, 56]. As former oxide, the binding energy does not change too much and remains at a low value [53]. This agrees with the faster degradation observed in the glasses with a higher content of PbO.

From the conservation point of view, glasses with a high content of lead and potassium should be identified as vulnerable due to their higher hygroscopicity and they should be maintained at moderately low humidity (40 - 45 % RH) [28, 57] to minimize the alteration rate.

5. Conclusions

Different accelerated corrosion tests were developed to determine the stability of high-lead glasses in aqueous and high-humidity environments. According to the results, in high-humidity environments, high-lead glasses adsorbed environmental water. Both, the adsorbed water and the aqueous solution produce the same alteration mechanism: first, the lixiviation of the alkali metal and lead ions, followed by the hydrolytic attack of the glass network due to the increase of the pH. High-lead glasses show the fastest degradation rate in contrast to glasses with higher

content of silica that are more stable. Environmental CO_2 can be dissolved in the aqueous medium forming bicarbonate and carbonate ions, depending on the pH of the medium that could precipitate in an environment with low humidity. In addition, the Pb^{2+}ions leached from the medium in basic solutions react quickly with the OH^- ions to form lead hydroxyl and carbonate complexes.

This study also confirms that it is important not to expose historical high-lead glasses to extremely high humidity (> 85 % RH) to avoid their alteration and to clean them with mixtures of water and solvents to favors their evaporation.

Acknowledgments

The authors acknowledge E. Peiteado, R. Navidad and S. Serena (ICV-CSIC, Spain) for their help during the tests, and the anonymous reviewers for their comments and suggestions that contributed to improve the final version of this paper. This work has been funded by Fundación General CSIC (ComFuturo Programme).

References

1. Henderson J, Warren SE. X-ray fluorescence analyses of Iron Age glass: Beads from Meare and Glastonbury lake villages. Archaeometry. 1981; 23(1): 83-94, doi: https://doi.org/10.1111/j.1475-4754.1981.tb00958.x.
2. Heck M, Hoffmann P. Coloured opaque glass beads of the Merovingians. Archaeometry. 2000; 42(2): 341-357, doi: https://doi.org/10.1111/j.1475-4754.2000.tb00886.x.
3. Welter N, Schüssler U, Kiefer W. Characterisation of inorganic pigments in ancient glass beads by means of Raman microspectroscopy, microprobe analysis and X-ray diffractometry. J. Raman Spectrosc. 2007; 38(1): 113-121, doi: https://doi.org/10.1002/jrs.1637.
4. Mecking O. Medieval lead glass in Central Europe. Archaeometry. 2013; 55(4): 640-662, doi: https://doi.org/10.1111/j.1475-4754.2012.00697.x.
5. Schibille N, Degryse P, Corremans M, Specht CG. Chemical characterisation of glass mosaic tesserae from sixth-century Sagalassos (south-west Turkey): chronology and production techniques. J. Archaeol. Sci. 2012; 39(5): 1480-1492, doi: https://doi.org/10.1016/j.jas.2012.01.020.
6. Bugoi R, Poll I, Mănucu-Adameşteanu G, Neelmeijer C, Eder F. Investigations of Byzantine glass bracelets from Nufăru, Romania using external PIXE–PIGE methods. J. Archaeol. Sci. 2013; 40(7): 2881-2891, doi: https://doi.org/10.1016/j.jas.2013.03.003.
7. Greiff S, Schuster J. Technological study of enamelling on Roman glass: The nature of opacifying, decolourizing and fining agents used with the glass beakers from Lübsow (Lubieszewo, Poland). J. Cult. Herit. 2008; 9: e27-e32, doi: https://doi.org/10.1016/j.culher.2008.06.006.
8. Henderson J. Chemical Characterization of Roman Glass Vessels, Enamels and Tesserae. MRS Proceedings. 1990; 185: 601, doi: https://doi.org/10.1557/PROC-185-601.
9. Palomar T, Oujja M, García-Heras M, Villegas MA, Castillejo M. Laser induced breakdown spectroscopy for analysis and characterization of degradation pathologies of Roman

glasses. Spectrochim. Acta B. 2013; 87: 114-120, doi: https://doi.org/10.1016/j.sab.2013.05.004.
10. Lahlil S, Cotte M, Biron I, Szlachetko J, Menguy N, Susini J. Synthesizing lead antimonate in ancient and modern opaque glass. J. Anal. Atom. Spectrom. 2011; 26(5): 1040-1050, doi: https://doi.org/10.1039/C0JA00251H.
11. Shortland AJ, Nicholson PT, Jackson CM. Lead isotopic analysis of eighteenth-dynasty Egyptian eyepaints and lead antimonate colourants. Archaeometry. 2000; 42(1): 153-157, doi: https://doi.org/10.1111/j.1475-4754.2000.tb00873.x.
12. Molina G, Odin GP, Pradell T, Shortland AJ, Tite MS. Production technology and replication of lead antimonate yellow glass from New Kingdom Egypt and the Roman Empire. J. Archaeol. Sci. 2014; 41: 171-184, doi: https://doi.org/10.1016/j.jas.2013.07.030.
13. Perea A. El tesoro visigodo de Guarrazar. Madrid: Editorial CSIC 2001.
14. Duckworth CN, de la Llave RC, Faber EW, Edwards DJG, Henderson J. Electron microprobe analysis of 9th–12th century islamic glass from Córdoba, Spain. Archaeometry. 2015; 57(1): 27-50, doi: https://doi.org/10.1111/arcm.12079.
15. de Juan Ares J, Schibille N. La Hispania antigua y medieval a través del vidrio: la aportación de la arqueometría. Bol. Soc. Esp. Ceram. V. 2017; 56(5): 195-204, doi: https://doi.org/10.1016/j.bsecv.2017.04.001.
16. Carmona N, Villegas MA, Jiménez P, Navarro J, García-Heras M. Islamic glasses from Al-Andalus. Characterisation of materials from a Murcian workshop (12th century AD, Spain). J. Cult. Herit. 2009; 10(3): 439-445, doi: https://doi.org/10.1016/j.culher.2008.12.005.
17. Kunicki-Goldfinger J, Madl M, Dzierzanowski P. Late 17th century glass vessels from Eiland-technological approach. In Michalik J, Smułek W, Godlewska-Para E (Eds.), Annual Report 2007. Warszawa, Poland: Institute of Nuclear Chemistry and Technology; 2007: p. 136-141.
18. Kunicki-Goldfinger J, Kierzek J, Kasprzak A, Małżewska-Bućko B. A study of eighteenth century glass vessels from central Europe by X-ray fluorescence analysis. X-Ray Spectrom. 2000; 29(4): 310-316, doi: https://doi.org/10.1002/1097-4539(200007/08)29:4<310::Aid-xrs431>3.0.Co;2-e.
19. Brain C. The technology of 17th century flint glass. In Proceedings of the XIX International Congress on Glass, Edinburgh, Scotland, 1–6 July 2001. 2002: p. 357-360.
20. Brain C, Brain S. The development of lead-crystal glass in London and Dublin: a reappraisal. Glass Technol. Part A. 2016; 57(2): 37-52, doi: https://doi.org/10.13036/1753-3546.57.2.015.
21. Di Febo R, Molera J, Pradell T, Melgarejo JC, Madrenas J, Vallcorba O. The production of a lead glaze with galena: Thermal transformations in the PbS–SiO_2 system. J. Am. Ceram. Soc. 2018; 101(5): 2119-2129, doi: https://doi.org/10.1111/jace.15346.
22. Salinas E, Pradell T, Molera J. Glaze production at an early Islamic workshop in al-Andalus. Archaeol. Anthrop. Sci. 2019; 11(5): 2201-2213, doi: https://doi.org/10.1007/s12520-018-0666-y.
23. Schalm O. Characterization of paint layers in stained-glass windows: main causes of the degradation of nineteenth century grisaille paint layers, PhD dissertation. Antwerp, Belgium: Universiteit Antwerpen; 2000.
24. Caen J. The production of stained glass in the County of Flanders and the Duchy of Brabant from the XVth to the XVIIIth centuries: materials and techniques. Belgium: Brepols; 2009.
25. Romero-Pastor J, Navarro JV, Egido Md, Ortega-Huertas M. A nondestructive methodology for the study of colored enamels: Insights into manufacturing and weathering processes. J. Am. Ceram. Soc. 2013; 96(7): 2132-2140, doi: https://doi.org/10.1111/jace.12402.

26. Machado C, Machado A, Palomar T, Vilarigues M. Grisaille in historical written sources. J. Glass Stud. 2019; 61: 71-86.
27. Merrifield MP. Medieval and Renaissance treatises on the arts of painting: original texts with English translations. New York: Dover Publications; 1999.
28. Brill RH. Crizzling – a problem in glass conservation. Stud. Conserv. 1975; 20(sup1): 121-134.
29. Kunicki-Goldfinger JJ. Identification of glass objects susceptible to crizzling. The case of Central European Baroque potassium glass. In Michalik J, Godlewska-Para E (Eds.), Annual Report 2018 Warszawa, Poland: Institute of Nuclear Chemistry and Technology; 2019: p. 79-80.
30. Wood S, Blachefe JR. Corrosion of lead glasses in acid media: II, concentration profile measurements. J. Am. Ceram. Soc. 1978; 61(7-8): 292-294, doi: https://doi.org/10.1111/j.1151-2916.1978.tb09311.x.
31. Wood S, Blachere JR. Corrosion of lead glasses in acid media: I, leaching kinetics. J. Am. Ceram. Soc. 1978; 61(7-8): 287-292, doi: https://doi.org/10.1111/j.1151-2916.1978.tb09310.x.
32. Lehman RL. Lead-ion stability in soda–lime lead silicate glasses. J. Am. Ceram. Soc. 1992; 75(8): 2194-2199, doi: https://doi.org/10.1111/j.1151-2916.1992.tb04483.x.
33. Kothiyal G, Phadnis S, Shrikhande V, Mirza T, Totlani M, Sahni V. A study of lead silicate glass degradation behaviour with reference to glass-to-metal seal applications. Anti-Corros. Method. M. 2000; 47(5): 280-285, doi: https://doi.org/10.1108/00035590010351503.
34. Cailleteau C, Weigel C, Ledieu A, Barboux P, Devreux F. On the effect of glass composition in the dissolution of glasses by water. J. Non-Cryst. Solids. 2008; 354(2): 117-123, doi: https://doi.org/10.1016/j.jnoncrysol.2007.07.063.
35. Rahimi RA, Sadrnezhaad SK, Raisali G. Chemical durability of lead silicate glass in HNO_3, HCl and H_2SO_4 aqueous acid solutions. J. Non-Cryst. Solids. 2009; 355(3): 169-174, doi: https://doi.org/10.1016/j.jnoncrysol.2008.11.001.
36. Rahimi RA, Sadrnezhaad SK. Effects of ion-exchange and hydrolysis mechanisms on lead silicate glass corrosion. Corrosion. 2012; 68(9): 793-800, doi: https://doi.org/10.5006/0528.
37. Zamora F. Biochemistry of alcoholic fermentation. In Moreno-Arribas MV, Polo C (Eds.), Wine Chemistry and Biochemistry. New York: Springer; 2009: p. 3-26.
38. Ahmed A, Youssof I. Reactions between water and lead crystal glass (24% PbO). Glass Technol. 1997; 38(1): 30-38.
39. Dungworth D, Brain C. Late 17th-century crystal glass: an analytical investigation. J. Glass Stud. 2009; 51: 111-137, doi: http://www.jstor.org/stable/24191233.
40. Schalm O, Van der Linden V, Frederickx P, Luyten S, Van der Snickt G, Caen J, et al. Enamels in stained glass windows: Preparation, chemical composition, microstructure and causes of deterioration. Spectrochim. Acta B. 2009; 64(8): 812-820, doi: https://doi.org/10.1016/j.sab.2009.06.005.
41. ISO 719:1985, Glass — Hydrolytic resistance of glass grains at 98 degrees C — Method of test and classification, 1985.
42. Palomar T, Chabas A, Bastidas DM, de la Fuente D, Verney-Carron A. Effect of marine aerosols on the alteration of silicate glasses. J. Non-Cryst. Solids. 2017; 471: 328-337, doi: https://doi.org/10.1016/j.jnoncrysol.2017.06.013.
43. Colomban P. Non–destructive Raman analysis of ancient glasses and glazes. In Janssens K (Ed.), Modern Methods for Analysing Archaeological and Historical Glass. University of Antwerp, Belgium: John Wiley & Sons, Ltd.; 2013: p. 275-300. https://onlinelibrary.wiley.com/doi/abs/10.1002/9781118314234.ch12
44. Bunker BC. Molecular mechanisms for corrosion of silica and silicate glasses. J. Non-Cryst. Solids. 1994; 179: 300-308, doi: https://doi.org/10.1016/0022-3093(94)90708-0.

45. Machado A, Vilarigues M. Blue enamel pigment—Chemical and morphological characterization of its corrosion process. Corros. Sci. 2018; 139: 235-242, doi: https://doi.org/10.1016/j.corsci.2018.05.005.
46. El-Batal FH, Khalil EMA, Hamdy YM, Zidan HM, Aziz MS, Abdelghany AM. Infrared reflection spectroscopy for precise tracking of corrosion behavior in 3d-transition metals doped binary lead silicate glass. Physica B. 2010; 405(12): 2648-2653, doi: https://doi.org/10.1016/j.physb.2010.03.044.
47. Palomar T, Llorente I. Decay processes of silicate glasses in river and marine aquatic environments. J. Non-Cryst. Solids. 2016; 449: 20-28, doi: https://doi.org/10.1016/j.jnoncrysol.2016.07.009.
48. Liu Q, Liu Y. Distribution of Pb(II) species in aqueous solutions. J. Colloid Interf. Sci. 2003; 268(1): 266-269, doi: https://doi.org/10.1016/S0021-9797(03)00638-6.
49. Wang Y-y, Chai L-y, Chang H, Peng X-y, Shu Y-d. Equilibrium of hydroxyl complex ions in Pb^{2+}-H_2O system. T. Nonferr. Metal. Soc. 2009; 19(2): 458-462, doi: https://doi.org/10.1016/S1003-6326(08)60295-2.
50. Palomar T. Effect of soil pH on the degradation of silicate glasses. Int. J. App. Glass Sci. 2017; 8(2): 177-187, doi: https://doi.org/10.1111/ijag.12226.
51. Falk M, Miller AG. Infrared spectrum of carbon dioxide in aqueous solution. Vib. Spectrosc. 1992; 4(1): 105-108, doi: https://doi.org/10.1016/0924-2031(92)87018-B.
52. ASM International Handbook Committee. ASM Handbook. United States: ASM International; 2004. https://books.google.es/books?id=W0dLAQAAIAAJ
53. Wang PW, Zhang L. Structural role of lead in lead silicate glasses derived from XPS spectra. J. Non-Cryst. Solids. 1996; 194(1): 129-134, doi: https://doi.org/10.1016/0022-3093(95)00471-8.
54. Rodrigues A, Fearn S, Vilarigues M. Historic K-rich silicate glass surface alteration: Behaviour of high-silica content matrices. Corros. Sci. 2018; 145: 249-261, doi: https://doi.org/10.1016/j.corsci.2018.10.010.
55. Rybicka A, Witkowska A, Bergmański G, Di Cicco A, Minicucci M, Mancini G. The structure of lead-silicate glasses: Molecular dynamics and EXAFS studies. J. Phys.-Condens. Mat. 2001; 13(43): 9781-9797, doi: https://doi.org/10.1088/0953-8984/13/43/309.
56. Morsi RMM, Ibrahim S, Morsi MM. Characterization of sodium lead silicate glasses containing low and high levels of Fe_2O_3 and effect of its replacement for Na_2O. J. Mater. Sci.- Mater. El. 2017; 28(13): 9566-9574, doi: https://doi.org/10.1007/s10854-017-6704-1.
57. Koob SP. Crizzling glasses: problems and solutions. Glass Technol. Part A. 2012; 53(5): 225-227.